1 **Title: "Genome-scale methods converge on key mitochondrial genes**

2 **for the survival of human cardiomyocytes in hypoxia."**

3 **Authors:** Lindsay M Edwards[a], Martin I Sigurdsson[b,c], Peter A Robbins[d], Michael E
4 Weale[e], Gianpiero L. Cavalleri[f], Hugh E Montgomery[g] and Ines Thiele[h]

5

6 **Affiliations:**
7 [a] School of Biomedical Science, King's College London, SE1 1UL, UK
8 [b] Department of Anaesthesia, Perioperative and Pain Medicine, Brigham and Women's
9 Hospital / Harvard Medical School, Boston, USA
10 [d] Department of Physiology, Anatomy and Genetics, University of Oxford, Oxford,
11 OX1 3PT, UK
12 [e] Department of Medical and Molecular Genetics, King's College London School of
13 Medicine, London, SE1 9RT, UK
14 [f] Molecular and Cellular Therapeutics, Royal College of Surgeons in Ireland, 123 St.
15 Stephen's Green, Dublin 2, Ireland
16 [g] Institute for Human Health and Performance, University College London, N19 5LW,
17 UK
18 [h] Luxembourg Centre for Systems Biomedicine, University of Luxembourg, Belval, 7,
19 avenue des Hauts-Fourneaux, L-4362 Esch-sur-Alzette, Luxembourg

20

21 ✉ **Address for Correspondence:**
22 Dr Lindsay Edwards
23 Centre of Human & Aerospace Physiological Sciences, King's College London
24 SH4.15 Guy's Campus
25 London SE1 1UL.
26 Tel: +44 (0)20 7848 6978
27 E-mail: lindsay.edwards@kcl.ac.uk
28
29 Running head: Constraint-based modelling, hypoxia and human genetics

30

31

32   **Abstract**

33   Background: Any reduction in myocardial oxygen delivery relative to its demands can

34   impair cardiac contractile performance. Understanding the mitochondrial metabolic

35   response to hypoxia is key to understanding ischemia tolerance in the myocardium.

36   We employed a novel combination of two genome-scale methods to study key

37   processes underlying human myocardial hypoxia tolerance. In particular, we

38   hypothesised that computational modelling and evolution would identify similar

39   genes as critical to human myocardial hypoxia tolerance. Methods & Results: We

40   analysed a reconstruction of the cardiac mitochondrial metabolic network using

41   constraint-based methods, under conditions of simulated hypoxia. We used flux

42   balance analysis, random sampling and principle components analysis to explore

43   feasible steady-state solutions. Hypoxia blunted maximal ATP (-17%) and haeme (-

44   75%) synthesis and shrank the feasible solution space. TCA and urea cycle fluxes

45   were also reduced in hypoxia, but phospholipid synthesis was increased. Using

46   mathematical optimization methods, we identified reactions that would be critical to

47   hypoxia tolerance in the human heart. We used data regarding SNP frequency and

48   distribution in the genomes of Tibetans (whose ancestors have resided in persistent

49   high-altitude hypoxia for several millennia). Six reactions were identified by both

50   methods as being critical to mitochondrial ATP production in hypoxia:

51   phosphofructokinase, phosphoglucokinase, Complex II, Complex IV, aconitase and

52   fumarase. Conclusions: Mathematical optimization and evolution converged on

53   similar genes as critical to human myocardial hypoxia tolerance. Our approach is

54   unique and completely novel and demonstrates that genome-scale modelling and

55   genomics can be used in tandem to provide new insights into cardiovascular genetics.

Introduction

Systems biology uses mathematical and computational methods to describe and explore complex biological networks. An important recent trend in systems biology has been the development and application of 'constraint-based modelling' [1]. Constraint-based modelling provides three very significant advantages over traditional mathematical approaches for the study of large and complex biochemical systems. First, very large models (up to thousands of reactions) can be accommodated. Thus the entire metabolic network of a mitochondrion (for example) can be modelled. Second, precise descriptions of the behaviour of each enzyme in the system (i.e. rate laws) are not required. Finally, detailed information regarding the activity of a single protein (for example, whether an enzyme is allosterically modified or not) is not necessary. Thus *unlike traditional 'kinetic' models, constraint-based models do not rely on, nor do they require, detailed knowledge of an enzyme's phosphorylation status (for example), nor the abundance of substrates and products.*

Constraint-based modelling is able to confer these advantages because the underlying models and assumptions are simple. The basic unit for constraint-based modelling is a *network model*, similar to the London Underground map. In the case of a biochemical network, this is constructed using 1) the known presence or absence of reactions based on genomic, proteomic or biochemical data; and 2) the known (species-specific) stoichiometry of all the chemical reactions included in the network. To this basic model are added a series of 'constraints' (from which the method derives its name), including reaction directionality, mass and charge balancing and absolute limits to metabolite uptake and excretion. Unlike traditional enzyme kinetic parameters (e.g. Michaelis-Menten midpoints), many of the underlying assumptions

81   in constraint-based models are robust to variations in physical environment (such as

82   temperature). However, constraint-based models are not able to simulate the exact

83   behaviour of a biochemical system. Instead, by keeping the underlying assumptions as

84   simple and robust as possible, they attempt to mirror the constraints which the true

85   network faces *in vivo*. Nevertheless, one can predict the most likely behaviour of the

86   system (using Monte Carlo methods) or predict the behaviour of the network at an

87   optimum value of some assumed 'physiological objective'. A more detailed

88   description of the approach can be found in the Methods and Supplemental Materials

89   of the present manuscript, and in many excellent reviews [1-4]. Regarding its utility:

90   constraint-based modelling, using genome-scale metabolic networks, has been used to

91   successfully predict the metabolic signatures of human inherited diseases [5-8], and to

92   permit the *in silico* design of tumour-specific toxins [9] and aid in the design of

93   microbial strains for the purposes of metabolic engineering [10].

94

95   Myocardial ischemia and hypoxia, whether cause or consequence, are common

96   features of the failing heart; understanding the mitochondrial response to hypoxia is

97   key to understanding ischemia tolerance. Myocardial hypoxia can be due to any

98   number of factors, but is most commonly caused by coronary artery or microvascular

99   heart disease, exacerbated by increased oxygen demand from ventricular remodelling.

100   Ischaemic heart disease remains the leading cause of death in the developed world;

101   therefore gaining new insights into the mechanisms whereby heart cells can survive

102   hypoxia of any duration is a matter of considerable importance.

103

104   Hypoxia, consequent upon a reduction in barometric pressure, is also a consistent

105   environmental challenge for human populations at high altitude, where it has led to a

106   robustly detectable degree of genetic and phenotypic divergence over evolutionary

107   timescales [11, 12]. Thus human populations at high altitude offer a unique opportunity to

108   study the genetic response to hypoxia. We used a novel combination of genome-scale

109   modelling, mathematical optimization and genome-wide analysis of single nucleotide

110   polymorphisms (SNPs) in humans to study the response of cardiac mitochondria to

111   hypoxia. In particular, we sought to test our hypothesis that if evolution is an

112   optimization process, then mathematical optimization methods, when applied to a

113   metabolic model, would converge on the same set of reactions, critical to

114   environmental (in this case hypoxic) performance. By comparing information from

115   natural (evolution) and mathematical optimization methods we sought to identify key

116   genes and reactions that underlie cardiac tolerance to hypoxia.

117

Methods

The reconstruction of the human cardiac mitochondrial metabolic network from proteomic and biochemical data was described previously [13]. Briefly, proteomic and transcriptomic data were used to derive an organelle 'metabolic parts list' (i.e. a list of all metabolic proteins known to be associated with a cardiac mitochondrion). These parts were 'connected' by their species-specific stoichiometric chemical equations. The draft reconstruction was extensively tested and manually curated. The final model used herein comprised 195 reactions, 235 metabolites and 25 exchange reactions (for a full description see [13, 14] and the Supplementary Materials). The exchange reactions did not represent genuine biochemical reactions, but instead described the exchanges that were necessary between the network and its environment so that a steady-state could be achieved. Having reconstructed the network, a series of limits or 'constraints' were added, all of which constrained the upper and lower limits of metabolite exchange of the model with its environment (e.g. oxygen, glucose). These constraints are in Supplementary Table 1 and represent maximum and minimum flux rates in human heart mitochondria *in vivo*. To simulate hypoxia, we reduced the upper constraint on oxygen uptake in the model to 25% of baseline values (normoxia), from 39.1 μM min^{-1} (g mitochondrial protein)$^{-1}$ (henceforth shortened to U) to 9.775 U. Our choice of simulating severe hypoxia was motivated by an intention to highlight any effects; however, it is worth noting that complete anoxia can occur in regions of ischemic myocardium (e.g. during acute myocardial infarction).

Computational analysis of network models rarely leads to a single set of predicted fluxes. Instead, methods are used to analyze the possible combinations of fluxes that allow a steady-state, given the applied constraints. The solutions together are termed

6

143   the feasible steady-state solution space. Alternatively, one can use linear optimization

144   to compute a set of fluxes that optimize the value of a given objective function, an

145   approach typically referred to as flux balance analysis (FBA). For example, this

146   method would return a set of fluxes that correspond to the highest possible rate of

147   ATP production by the network, if ATP production was the objective function. When

148   conducting FBA, we optimized the mitochondrial network for three objective

149   functions (phospholipid, haeme and ATP synthesis) [13]. Alternate optimal solutions

150   (i.e. other sets of fluxes that also gave an optimal objective) were accounted for via

151   flux variability analysis (see below). We also studied the optimization of all three

152   objectives simultaneously (see Supplementary Materials for details). This method

153   comprises placing the objective functions under study into hierarchical order (for

154   example, haeme biosynthesis then phospholipid biosynthesis then ATP synthesis).

155   The network is optimized for the first objective, then optimized for the second with

156   the first held at optimal value and so forth.

157

158   We used two computational methods to identify reactions that are critical to hypoxia

159   tolerance in the mitochondria metabolic network – shadow prices [15] and flux spans [16].

160   Shadow prices have been used in metabolic network analysis before [15, 17]. Shadow

161   prices (also known as Lagrange multipliers) are measures of the degree to which the

162   value of the objective function is affected by the availability of a particular resource.

163   For example, if ATP synthesis were the objective function, a shadow price of 1.0 for

164   glucose (for example) would indicate that a 1 unit increase in glucose availability

165   would lead to an equivalent increase in ATP synthesis. A shadow price of 2.0 would

166   indicate that a unit increase in the availability of glucose would result in a two unit

167   increase in ATP synthesis, and so forth. We reasoned therefore that reactions for

168   which metabolites with large, positive shadow prices were either substrates or

169   products, would be crucial to hypoxic performance (at least, for the objective function

170   under investigation). To assess the likelihood that our method had outperformed

171   chance, we used simple permutation testing.

172

173   Our second approach was to use flux spans. Using flux variability analysis [18] we

174   computed the range of values that flux through each reaction could take at an

175   optimum (computed using FBA). Taken together, these ranges delineate the set of

176   alternate optimal solutions (i.e. different sets of fluxes that result in the same optimal

177   value of the objective) [18]. By calculating the difference between the upper and lower

178   feasible fluxes we derived a flux span for each reaction. Here we express these as a

179   relative ratio. Hence a reaction with flux = 10 U and with the lower and upper feasible

180   fluxes being 8 and 12 U respectively would have a relative flux span of 0.4 (or 40%).

181   We reasoned that reactions with the smallest relative flux spans would be critical to

182   hypoxia tolerance and hypoxic performance. Again, we used permutations to estimate

183   the probability that our method had outperformed chance alone.

184

185   We used data from a genome-wide allelic differentiation scan (GWADS) comparing

186   SNP frequencies of Tibetans ($n = 35$) residing at 3200-5000 m, with 84 individuals

187   from the founder population. Subjects were recruited from three distinct regions of

188   China: the North Western region of Yunnan province, Mag Xiang and Zhaxizong

189   Xiang (both in the Tibet Autonomous Region). Genotypic data from the HapMap

190   Phase III Han population were also included. These data have been analyzed

191   previously[11] and full details can be found in this earlier publication. Each gene was

192   assigned a genome-wide p-value that serves as an estimate of the degree of selective

193   pressure applied to that gene (through differences in SNP frequency). Details

194   regarding the calculation of these *p*-values can also be found elsewhere [11]. We

195   extracted the *p*-values corresponding to the genes in our model and ranked genes by

196   smallest GWADS *p*-value first, producing a list of nuclear-encoded mitochondrial

197   genes with an accompanying measure of selective pressure in humans living in

198   persistent hypoxia.

199

200   Where appropriate, means and standard deviations are given. However, modelling

201   results are often a single datum point (e.g. differences in optimal ATP synthesis rate,

202   determined using flux balance analysis, under hypoxia and normoxia) and are

203   therefore given as such.

204

205

Results

We optimized the network for three physiological 'targets' (objective functions) -

ATP, haeme and phospholipid biosynthesis [13] – using flux balance analysis (FBA) [1].

Hypoxia reduced the optimal ATP synthesis rate by 13%, from 45.8 to 36.6 U. Figure

1 shows a quantized heatmap of the accompanying differences in flux. There were

reductions in flux through many reactions comprising the TCA cycle and oxidative

phosphorylation. There were also reductions in flux through most reactions

comprising fatty acid uptake, transport, activation and oxidation, although some were

maintained due to the imposition of a minimum uptake rate (this is a physiological

constraint imposed by the ability of fatty acids to diffuse freely across membranes).

Glycolytic rates were similar, which was expected as maximal ATP synthesis was the

objective. The flux through multiple reactions required for phospholipid biosynthesis

were increased and the demand reaction was activated in hypoxia. To ensure that the

degree of simulated hypoxia affected our results quantitatively but not qualitatively,

we performed additional flux balance analysis experiments at various intermediate

oxygen uptake rates. The results are in Supplementary Figure 1. Briefly, maximal

ATP synthesis was progressively reduced by increasing hypoxia. Consistent with our

interpretation, phospholipid biosynthesis was not activated until O_2 uptake dropped

below a critical level, at which point a 'sink' for fatty acid carbons was required.

There was no evidence of qualitative shifts in carbon flux as maximal O_2 uptake rate

was progressively reduced.

Haeme synthesis was blunted by 75% in hypoxia (hypoxia: 0.650 vs. normoxia: 2.44

U). The pattern of flux differences between the optimized network in normoxia and

hypoxia was similar to that with ATP synthesis as the objective. Flux through

231 reactions comprising the TCA cycle, oxidative phosphorylation, the urea cycle and

232 haeme synthesis itself were suppressed. There were increases in long-chain (C20:4

233 and C22:6) activation and an increase in phospholipid biosynthesis. A heatmap of

234 differences in flux across the network under these conditions (haeme biosynthesis as

235 the objective function in hypoxia vs. normoxia) is given in Supplementary Figure 2.

236 However, when phospholipid biosynthesis was the objective it was unchanged by

237 oxygen restriction, at 22.8 U.

238

239 We then performed multiple objective analyses with three different hierarchies of

240 objective functions. 1. ATP > haeme > phospholipid: In normoxia, and with ATP

241 synthesis fixed at its optimal value of 45.8 U, haeme and phospholipid synthesis were

242 eliminated. In hypoxia, with ATP synthesis fixed at its optimal value of 36.6 U,

243 haeme synthesis was still eliminated; however, optimized phospholipid biosynthesis

244 was now non-zero, although reduced ~100-fold at 0.265 U. 2. Haeme > phospholipid

245 > ATP: In normoxia, with haeme biosynthesis at its optimal rate of 2.44 U, both

246 phospholipid and ATP synthesis were abolished. In hypoxia, with haeme biosynthesis

247 at 0.650, phospholipid biosynthesis was possible and optimized to 0.867 U; ATP

248 synthesis was abolished. 3. Phospholipid > haeme > ATP: As maximal phospholipid

249 biosynthesis was unaffected by hypoxia it was fixed at 0.867 U for both conditions

250 (normoxia/hypoxia). In both normoxia and hypoxia, haeme biosynthesis gained

251 optimal values the same as those where it was the only objective function considered

252 (normoxia: 2.44 U vs. hypoxia: 0.650 U). In normoxia, ATP biosynthesis was

253 subsequently limited to 8.85 U; in hypoxia it was reduced far less, to 19.3 U. A

254 summary of all the optima is in Supplementary Table 2.

255

256   We next used uniform random sampling [19], a method that characterizes the steady-

257   state solution space without requiring an objective function. Figure 1b shows a

258   quantized heatmap of differences in median flux. Consistent with the FBA results,

259   fluxes through reactions comprising oxidative phosphorylation, the TCA cycle and

260   fatty acid metabolism were reduced in hypoxia. Without the requirement to maximize

261   ATP synthesis in normoxia that was elsewhere imposed by FBA, glycolytic flux

262   increased in hypoxia. The heatmap shows a reduction in flux through lactate

263   dehydrogenase and the lactate transporter; however, this represents a *reversal* in flux,

264   from uptake to efflux. Also noteworthy is a reduction in urea cycle flux in hypoxia.

265

266   We analysed the sampled data using principal components analysis (PCA), allowing

267   us to visualize patterns of change. We modelled the sampled data together and found

268   that five components captured 65% of the total variance. When plotted, the scores on

269   these components revealed that hypoxia substantially reduced the dimensions of the

270   solution space, reducing the flexibility of the metabolic network even though the

271   dimensions of the space were the same. This was especially apparent in principal

272   components 1 and 2 (Figure 2), with principal component 1 being dominated by

273   reactions related to gas exchange, the TCA cycle and oxidative phosphorylation and

274   principal component 2 being dominated by reactions related to iron transport and

275   haeme biosynthesis.

276

277   Given that optimal phospholipid biosynthesis was unaffected by oxygen restriction,

278   we continued by studying those metabolites and reactions that limited optimal ATP

279   and haeme biosynthesis in the mitochondrial metabolic network under hypoxia. We

280   first computed shadow prices for all metabolites in the model when optimising the

281 network for either ATP or haeme synthesis. Table 2 gives metabolites with the largest

282 positive shadow prices and the corresponding twenty discrete reactions for each

283 objective function. Three classes of metabolite (and reaction) dominated: long-chain

284 (>20C) fatty acid transport, glycolysis and haeme biosynthesis. When optimising for

285 ATP synthesis, the largest shadow prices were several-fold larger than when

286 optimising for haeme synthesis (e.g. 4.0 for cytosolic fructose diphosphate, fdp(c), vs.

287 1.2 for cytosolic arachidonic acid, c206(c)). When optimizing the network with ATP

288 synthesis as the objective function, the metabolites with large positive shadow prices

289 were mainly related to glycolysis, oxidative phosphorylation and the TCA cycle.

290

291 We next computed flux spans, using flux variability analysis. The reactions with the

292 smallest relative flux spans when optimizing the network for either haeme or ATP

293 synthesis are given in Table 3. As with shadow prices, the magnitude of the parameter

294 (in this case, relative flux span) was several fold different when optimizing ATP vs.

295 haeme synthesis; in both cases the difference (larger shadow prices and smaller flux

296 spans) was consistent with ATP synthesis being more tightly restricted by hypoxia.

297 Interestingly, reactions related to oxidative phosphorylation both had narrow flux

298 spans regardless of whether ATP or haeme synthesis were the objectives. In particular,

299 complex IV of the respiratory chain was ranked in the top two (Table 3). Perhaps

300 unsurprisingly, reactions related to proto-haeme synthesis and iron transport also had

301 small relative flux spans when optimizing for haeme synthesis. When optimizing the

302 network for ATP synthesis, reactions from the TCA cycle and glycolysis were highly

303 represented.

304

305 We generated a complete list of nuclear-encoded mitochondrial genes with a

306 corresponding measure of selective pressure at high altitude. The twenty 'most

307 selected' genes (i.e. smallest p-value) are in Table 1. Using permutations, we assessed

308 the likelihood that mathematical optimization had outperformed chance when

309 predicting genes under pressure. When conducting shadow price analysis with ATP

310 synthesis as the objective, we selected the 16 metabolites with the largest positive

311 shadow price corresponding to 20 discrete reactions shown in Table 2. Of these 20

312 reactions, two (phosphofructokinase (PFK) and phosphoglycerate kinase (PGK))

313 carried flux and corresponded to genes in Table 1. However, permutation testing

314 suggested that random selections of 16 metabolites would equal or outperform our

315 modelling approach most of the time (p = ~0.860). We observed that two of the only

316 three metabolites with shadow prices of 3 or greater when optimizing the network for

317 either objective (cytosolic fructose 6-phosphate and fructose diphosphate, f6p(c) and

318 fdp(c) respectively in Table 2) are both substrate and product for PFK, the most

319 'heavily selected' gene in Table 1. We next compared the reactions highlighted by

320 shadow price analysis whilst optimizing the network for haeme synthesis. Three

321 reactions were common with those in Table 1: hydroxymethylbilane synthase

322 (HMBS), porphobilinogen synthase (PPBNGS) and phosphoglycerate kinase (PGK).

323 Once again, permutations suggested that shadow pricing had not outperformed chance

324 when identifying genes under pressure.

325

326 We used a similar approach to assess the performance of flux span analysis. Table 3

327 shows that flux span analysis identified three (haeme synthesis) and six (ATP

328 synthesis) reactions that were common with those that were the most heavily selected

329 genes in Table 1. With ATP synthesis as the objective, we used permutation testing to

330 assess whether modelling had outperformed chance when predicting genes under

331   pressure. Random selections only matched flux span analysis 1675 out of 100000

332   times, offering evidence that this approach had outperformed chance at $p < .05$.

333

334   We repeated this process with haeme synthesis as the objective function. Using

335   100000 permutations, random selection matched the model performance

336   approximately half the time (p = ~0.525). Hence using flux span analysis with haeme

337   as the objective had not outperformed chance.

338 **Discussion**

339 Myocardial hypoxia can be either acute or chronic and occurs whenever oxygen

340 delivery is insufficient to meet the needs of the contracting myocardium. This can be

341 due to any combination of reduced O_2-carrying capacity due to anaemia, reduced

342 haemoglobin saturation (whether environmental or pathological), poor cardiac output

343 or compromised blood flow due to coronary artery or microvascular heart disease, and

344 increased oxygen demand associated with stress or structural remodelling (e.g.

345 ventricular hypertrophy). Ischaemic heart disease remains the leading cause of death

346 in the developed world. A notable feature of heart failure is that, once left ventricular

347 dysfunction has been established, patients suffer a relentless apoptotic loss of viable

348 cardiomyocytes that some investigators believe to be due to repeated, transient

349 ischaemic and hypoxic events [20]. Therefore understanding the mechanisms whereby

350 heart cells can survive either transient or sustained hypoxia and ischaemia is a matter

351 of considerable importance. Here we present an entirely new approach to this question

352 using systems biology methods that encompass genomics, metabolic modelling and

353 mathematical optimization.

354

355 We first studied the effect that hypoxia had on the solution space (the set of all

356 feasible fluxes) of the reconstructed cardiac mitochondrial metabolic network using

357 two complementary methods – optimization (FBA) and Monte Carlo sampling.

358 Optimization requires an objective function; in keeping with previous work we

359 studied three objectives that are central to mitochondrial function: the synthesis of

360 ATP, haeme and mixed phospholipids [13]. Although maximal phospholipid synthesis

361 was unaffected by hypoxia, both haeme and ATP synthesis were reduced (by 75% and

362 13% respectively). The reduction in maximal ATP synthesis was accompanied by

363 reductions in TCA cycle flux, oxidative phosphorylation and fatty acid uptake and

364 processing but a seemingly paradoxical increase in phospholipid biosynthesis.

365

366 The degree to which maximal haeme synthesis was blunted in hypoxia was striking.

367 This 75% loss of proto-haeme synthesis capacity was accompanied by many of the

368 metabolic features observed when optimizing ATP production in hypoxia. Haeme is a

369 major component of haemoglobin, itself substantially increased in response to

370 hypoxia to enhance systemic oxygen transport [21]. Thus network stoichiometry forms a

371 constraint to haeme biosynthesis that may partly define the speed with which haeme

372 can be synthesized in hypoxia. Non iron-deficient anaemia is a common feature in

373 heart failure patients, yet its aetiology is unknown [22]. Furthermore, many studies have

374 shown that reduced haemoglobin is an independent predictor of risk in heart failure

375 patients [23, 24], although again the mechanism remains poorly understood. Our

376 simulations suggest that hypoxia itself can cause significant reductions in proto-

377 haeme synthesis, both in the heart and elsewhere, and that hypoxia of any kind could

378 lead to a vicious cycle of blunted haeme synthesis, reduced O_2-carrying capacity in

379 blood and subsequently worsened hypoxaemia. Furthermore, in cultured human

380 neurons, haeme deficiency causes a decrease in (haeme-containing) complex IV

381 (cytochorome c oxidase) and activation of nitric oxide synthase [25]. Given that

382 complex IV release is a key component of the p53 apoptotic cascade [26], this suggests

383 an intriguing new avenue for investigations into hypoxia-induced myocyte apoptosis.

384

385 We studied the effect on mitochondria of forcing them to balance competing

386 objectives in hypoxia. When ATP production was given hierarchical 'superiority' (as

387 is almost certainly the case *in vivo*), haeme synthesis was completely abolished in

388   normoxia and hypoxia. Thus haeme and ATP synthesis compete for the same

389   resources; quite moderate reductions in O_2 supply, coupled with increases in ATP

390   demand, might lead to profound reductions in haeme synthesis capacity due to

391   stoichiometric constraints in the metabolic network. Interestingly, phospholipid

392   biosynthesis was abolished in normoxia under this hierarchy but was active in

393   hypoxia. This was likely due to competition with ATP synthesis for lipids; in hypoxia,

394   ATP synthesis was diminished freeing up lipids for phospholipid synthesis.

395

396   We next studied the set of feasible solutions using random sampling. Multiple random

397   samples of the solution space allow the generation of probability density functions for

398   flux through every reaction; the most probable value can often predict the measured *in*

399   *vivo* rate [14]. As with linear optimization (FBA) we observed reductions in TCA cycle

400   and oxidative phosphorylation reactions, in addition to a reduction in urea cycle flux.

401   This last is intriguing because flux through arginosuccinate synthetase (*ASS*) was

402   decreased in simulated hypoxia. *ASS* been elsewhere been reported as a target of the

403   von Hippel-Lindau tumour suppressor gene (*VHL*) [27], an inverse regulator of HIF-1α.

404   Manipulation of *VHL* expression led to corresponding changes in ASS levels in

405   RCC10 renal cell carcinoma cells.

406

407   Once again we observed that many of the reactions required for phospholipid

408   biosynthesis were increased and the biosynthesis reaction itself was activated in

409   hypoxia. Without this redirection of fatty acid flux, the imposition of hypoxia,

410   combined with minimum uptake rates for fatty acids, would have led to an

411   accumulation of unoxidized fatty acids in the model and a loss of homeostasis.

412   Cardiac mitochondria face an identical challenge *in vivo* and redirect fatty acids to

413 storage (away from oxidation) when ischaemic [28]. Similarly, Langendorff-perfused

414 hearts exposed to acute hypoxia increase phospholipid biosynthesis to maintain lipid

415 homeostasis [29]. We also observed an increase in glycolytic flux (Figure 1B).

416

417 Overall, the pattern of change in metabolic flux in our simulations was strikingly

418 consistent with experimental observations of cellular responses to hypoxia, including

419 the reduction in flux through pyruvate dehydrogenase (PDHm) *in vivo* that is brought

420 about by modulation of pyruvate dehydrogenase kinase [30]. It is interesting to note that

421 the reduction in flux through PDHm in our simulations directly resulted from network

422 stoichiometry, without any additional explanation or control. While the notion that

423 glycolytic flux is increased in hypoxia is certainly not new, altered (particularly

424 increased) lipid biosynthesis in response to hypoxia is a less often considered

425 component of hypoxia tolerance. Previous investigators have reported both increased

426 [29, 31] and decreased [32] lipid synthesis in hypoxia in model systems. These

427 discrepancies may be due to differences in isotope labelling strategy (e.g. acetate vs.

428 glycerol vs. palmitate) or outcome measure. However, there is no question that lipids

429 accumulate in the heart in response to hypoxia and ischaemia [28]. It should be noted

430 that the details of whole heart lipid-handling in hypoxia and/or ischemia may be

431 different to the mitochondrial response considered in isolation. It is interesting also

432 that lipotoxicity – defined as a chronic mismatch between oversupply of acetyl-CoA

433 from lipid breakdown and its subsequent mitochondrial oxidation – is a stoichiometric

434 disorder and can be as readily caused by impaired oxidative phosphorylation (for

435 example, by hypoxia) as lipid oversupply. The consistency of our simulations with

436 experimental observations reinforced to us the notion that our methods were both

437 robust and relevant.

438

439 We sought to test whether mathematical optimization had converged on the same

440 reactions that human evolution had identified as being critical to optimal hypoxic

441 function. We used data from a GWADS scan comparing SNP frequencies of Tibetans

442 residing at 3500 m (and whose ancestors have 'lived high' for over 10,000 years [33])

443 with individuals from the HapMap Phase III Chinese Han sample, who are closely

444 related but have resided at sea level throughout [11]. Tibetans were ideal for this study

445 because, despite systemic adjustments (for example, increased breathing rates), they

446 continue to have lower arterial oxygen content than sea-level dwellers [34].

447

448 It is interesting that the largest shadow prices were recorded when optimizing the

449 mitochondrial metabolic network for ATP synthesis in hypoxia. This suggests that,

450 even in the case of competing objectives, increasing the supply of these metabolites

451 would be especially advantageous when oxygen supply is limited (either by

452 environment or pathology). The metabolite with the largest shadow price in any

453 analysis we conducted was fructose diphosphate, a product of phosphofructokinase

454 (PFK). However, permutation testing failed to support the notion that shadow prices

455 and evolution had converged on similar reactions.

456

457 The results gained by examining flux spans were more compelling. Flux spans are the

458 range of values within which a reaction rate can lie at a computed optimum. We

459 reasoned that reactions with narrow flux spans would be under greater selective

460 pressure. We generated a list of reactions with the smallest flux spans (yet which

461 carried flux) and compared these with the SNP data. When we optimized for ATP

462 synthesis, the results supported the notion that mathematical optimization and

463   evolution had converged on similar reactions (where 6/20 reactions were common

464   between the two selections). The common reactions selected by flux span analysis and

465   evolution were related to haeme synthesis (although only when optimizing for haeme

466   synthesis), glycolysis (PFK, PGK), the TCA cycle (aconitase and fumarase) and

467   oxidative phosphorylation (Complexes II and IV). We propose that our combined

468   method has identified reactions that are especially important in maintaining or

469   increasing mitochondrial ATP synthesis in the hypoxic heart. This view is supported

470   by the existing literature. For example, it was recently reported that mice exposed to

471   three weeks of normobaric hypoxia had reduced Complex II, IV and aconitase activity

472   in cardiac mitochondria [35] while fumarate accumulation leads to 'pseudo-hypoxic'

473   activation of HIF-1α [36], suggesting that many of the same reactions highlighted here

474   indeed have important roles in hypoxic adaptation and, hence, survival. Our combined

475   approach also yielded an unexpected benefit: Computational analysis was able to

476   provide suggestions as to whether genes were under positive or negative selective

477   pressure (an important distinction to which traditional genome-wide analytical

478   techniques are blind).

479

480   A final note regarding PFK: basic biochemistry textbooks all highlight the importance

481   of PFK as a key regulatory step in glycolysis (e.g. page 444 in [37]). Yet there is a

482   tautology here: PFK is heavily regulated biologically (for example, by ATP/AMP,

483   fructose 2,6-bisphosphate [37] etc.). However its heavy regulation is evidence for, not an

484   explanation of, its importance. We note that in our simulations, using multiple

485   objectives and alternative analytical strategies, PFK was repeatedly highlighted as

486   being an important determinant of the objective. Our model contained no information

487   whatsoever regarding biological regulation (for example, allosteric modulation by

488   other small molecules). In other words, our simulations suggest that PFK is important

489   because it occupies a critical point in the metabolic network due to network topology

490   and nothing more. By extension, this protein is likely to be under strong evolutionary

491   selective pressure in many environments, leading to complex phenotypic properties.

492   Once again this was supported in the genetic data, at least in hypoxia.

493

494   *Limitations*

495   Our main hypothesis - that evolution and mathematical optimization would converge

496   on similar targets – was supported. In so doing we generated a list of genes that the

497   two methods independently highlighted as potentially important for hypoxic survival.

498   Although we believe that the nature of our combined approach adds additional

499   support to the significance of these genes, we wish to stress that genes identified by

500   any genome-wide method should be treated as 'candidates' only. Direct experimental

501   evidence will always be required to clarify the function of each. Of course, for some

502   of the genes identified by our approach, overwhelming evidence already exists

503   confirming their importance (for example, pyruvate dehydrogenase [30, 38, 39]).

504

505   A second limitation relates to possible differences in the Han vs. Tibetan environment

506   beyond simply altitude (e.g. diet and temperature). Several points are pertinent:

507   1. Although temperatures may differ between the two locations, most very high

508   altitude populations descend lower in winter;

509   2. Diet may differ; however many essential elements (reliance on vegetables and use

510   of rice) are similar;

511   3. Multiple studies have utilized the Han vs Tibetan genome comparison. All have

512   found the same primary hit (EPAS1), which is a gene regulating expression of a

513   hypoxia-responsive transcription factor;

514   4. The candidates in the present study were chosen because computational analysis of

515   a separate network model suggested their role in hypoxia. This makes it more likely

516   that this was indeed the cause and is, potentially, another benefit of our approach.

524   **References**

525   1.   Lewis NE, Nagarajan H, Palsson BO. Constraining the metabolic genotype-

526   phenotype relationship using a phylogeny of in silico methods. *Nat Rev*

527   *Microbiol*. 2012;10:291-305

528   2.   Bordbar A, Palsson BO. Using the reconstructed genome-scale human

529   metabolic network to study physiology and pathology. *J Intern Med*.

530   2012;271:131-141

531   3.   Oberhardt MA, Palsson BO, Papin JA. Applications of genome-scale

532   metabolic reconstructions. *Mol Syst Biol*. 2009;5:320

533   4.   Edwards LM, Thiele I. Applying systems biology methods to the study of

534   human physiology in extreme environments. *Extreme Phys Med*. 2013;2

535   5.   Sigurdsson MI, Jamshidi N, Jonsson JJ, Palsson BO. Genome-scale network

536   analysis of imprinted human metabolic genes. *Epigenetics*. 2009;4:43-46

537   6.   Smith AC, Robinson AJ. A metabolic model of the mitochondrion and its use

538   in modelling diseases of the tricarboxylic acid cycle. *BMC Syst Biol*.

539   2011;5:102

540   7.   Shlomi T, Cabili MN, Ruppin E. Predicting metabolic biomarkers of human

541   inborn errors of metabolism. *Mol Syst Biol*. 2009;5:263

542   8.   Thiele I, Swainston N, Fleming RMT, Hoppe A, Sahoo S, Aurich MK,

543   Haraldsdottir H, Mo ML, Rolfsson O, Stobbe MD, Thorleifsson SG, Agren R,

544   Bolling C, Bordel S, Chavali AK, Dobson P, Dunn WB, Endler L, Hala D,

545   Hucka M, Hull D, Jameson D, Jamshidi N, Jonsson JJ, Juty N, Keating S,

546   Nookaew I, Le Novere N, Malys N, Mazein A, Papin JA, Price ND, Selkov E,

547   Sigurdsson MI, Simeonidis E, Sonnenschein N, Smallbone K, Sorokin A, van

548   Beek JHGM, Weichart D, Goryanin I, Nielsen J, Westerhoff HV, Kell DB,

549   Mendes P, Palsson BO. A community-driven global reconstruction of human

550   metabolism. *Nat Biotech*. 2013;advance online publication

551   9.   Frezza C, Zheng L, Folger O, Rajagopalan KN, MacKenzie ED, Jerby L,

552   Micaroni M, Chaneton B, Adam J, Hedley A, Kalna G, Tomlinson IP, Pollard

553   PJ, Watson DG, Deberardinis RJ, Shlomi T, Ruppin E, Gottlieb E. Haem

554   oxygenase is synthetically lethal with the tumour suppressor fumarate

555   hydratase. *Nature*. 2011;477:225-228

556 10. Hua Q, Joyce AR, Fong SS, Palsson BO. Metabolic analysis of adaptive

557   evolution for in silico-designed lactate-producing strains. *Biotechnol Bioeng*.

558   2006;95:992-1002

559 11. Beall CM, Cavalleri GL, Deng L, Elston RC, Gao Y, Knight J, Li C, Li JC,

560   Liang Y, McCormack M, Montgomery HE, Pan H, Robbins PA, Shianna KV,

561   Tam SC, Tsering N, Veeramah KR, Wang W, Wangdui P, Weale ME, Xu Y,

562   Xu Z, Yang L, Zaman MJ, Zeng C, Zhang L, Zhang X, Zhaxi P, Zheng YT.

563   Natural selection on epas1 (hif2alpha) associated with low hemoglobin

564   concentration in tibetan highlanders. *Proc Natl Acad Sci U S A*.

565   2010;107:11459-11464

566 12. Yi X, Liang Y, Huerta-Sanchez E, Jin X, Cuo ZX, Pool JE, Xu X, Jiang H,

567   Vinckenbosch N, Korneliussen TS, Zheng H, Liu T, He W, Li K, Luo R, Nie

568   X, Wu H, Zhao M, Cao H, Zou J, Shan Y, Li S, Yang Q, Asan, Ni P, Tian G,

569   Xu J, Liu X, Jiang T, Wu R, Zhou G, Tang M, Qin J, Wang T, Feng S, Li G,

570   Huasang, Luosang J, Wang W, Chen F, Wang Y, Zheng X, Li Z, Bianba Z,

571   Yang G, Wang X, Tang S, Gao G, Chen Y, Luo Z, Gusang L, Cao Z, Zhang Q,

572   Ouyang W, Ren X, Liang H, Huang Y, Li J, Bolund L, Kristiansen K, Li Y,

573   Zhang Y, Zhang X, Li R, Yang H, Nielsen R, Wang J. Sequencing of 50

574   human exomes reveals adaptation to high altitude. *Science*. 2010;329:75-78

575 13. Vo TD, Greenberg HJ, Palsson BO. Reconstruction and functional

576   characterization of the human mitochondrial metabolic network based on

577   proteomic and biochemical data. *J Biol Chem*. 2004;279:39532-39540

578 14. Thiele I, Price ND, Vo TD, Palsson BO. Candidate metabolic network states

579   in human mitochondria. Impact of diabetes, ischemia, and diet. *J Biol Chem*.

580   2005;280:11683-11695

581 15. Savinell JM, Palsson BO. Network analysis of intermediary metabolism using

582   linear optimization. I. Development of mathematical formalism. *J Theor Biol*.

583   1992;154:421-454

584 16. Ghosh A, Zhao H, Price ND. Genome-scale consequences of cofactor

585   balancing in engineered pentose utilization pathways in *saccharomyces*

586   *cerevisiae*. *PLoS ONE*. 2011;6:e27316

587 17. Varma A, Boesch BW, Palsson BO. Stoichiometric interpretation of

588   escherichia coli glucose catabolism under various oxygenation rates. *Appl*

589   *Environ Microbiol*. 1993;59:2465-2473

590 18. Mahadevan R, Schilling CH. The effects of alternate optimal solutions in

591   constraint-based genome-scale metabolic models. *Metabolic engineering*.

592   2003;5:264-276

593 19. Kaufman DE, Smith RL. Direction choice for accelerated convergence in hit-

594   and-run sampling. *Operations Research*. 1998;46:84-95

595 20. Sabbah HN, Sharov VG, Goldstein S. Cell death, tissue hypoxia and the

596   progression of heart failure. *Heart Fail Rev*. 2000;5:131-138

597   21.   Martin D, Windsor J. From mountain to bedside: Understanding the clinical

598   relevance of human acclimatisation to high-altitude hypoxia. *Postgrad Med J.*

599   2008;84:622-627; quiz 626

600   22.   Coats AJ. Anaemia and heart failure. *Heart*. 2004;90:977-979

601   23.   Sharma R, Francis DP, Pitt B, Poole-Wilson PA, Coats AJS, Anker SD.

602   Haemoglobin predicts survival in patients with chronic heart failure: A

603   substudy of the elite ii trial. *European Heart Journal*. 2004;25:1021-1028

604   24.   Go AS, Yang J, Ackerson LM, Lepper K, Robbins S, Massie BM, Shlipak

605   MG. Hemoglobin level, chronic kidney disease, and the risks of death and

606   hospitalization in adults with chronic heart failure: The anemia in chronic

607   heart failure: Outcomes and resource utilization (anchor) study. *Circulation*.

608   2006;113:2713-2723

609   25.   Atamna H, Killilea DW, Killilea AN, Ames BN. Heme deficiency may be a

610   factor in the mitochondrial and neuronal decay of aging. *Proc Natl Acad Sci U*

611   *S A*. 2002;99:14807-14812

612   26.   Schuler M, Bossy-Wetzel E, Goldstein JC, Fitzgerald P, Green DR. P53

613   induces apoptosis by caspase activation through mitochondrial cytochrome c

614   release. *Journal of Biological Chemistry*. 2000;275:7337-7342

615   27.   Harten SK, Esteban MA, Maxwell PH. Identification of novel vhl regulated

616   genes by transcriptomic analysis of rcc10 renal carcinoma cells. *Adv Enzyme*

617   *Regul*. 2009;49:43-52

618   28.   Scheuer J, Brachfeld N. Myocardial uptake and fractional distribution of

619   palmitate-1 c14 by the ischemic dog heart. *Metabolism*. 1966;15:945-954

620   29.   Chabowski A, Gorski J, Calles-Escandon J, Tandon NN, Bonen A. Hypoxia-

621   induced fatty acid transporter translocation increases fatty acid transport and

622   contributes to lipid accumulation in the heart. *FEBS Lett*. 2006;580:3617-3623

623   30.   Kim JW, Tchernyshyov I, Semenza GL, Dang CV. Hif-1-mediated expression

624   of pyruvate dehydrogenase kinase: A metabolic switch required for cellular

625   adaptation to hypoxia. *Cell Metab*. 2006;3:177-185

626   31.   Harris P, Gloster J. The effects of acute hypoxia on lipid synthesis in the rat

627   heart. *Cardiology*. 1971;56:43-47

628   32.   Cheng P, Hatch GM. Inhibition of cardiolipin biosynthesis in the hypoxic rat

629   heart. *Lipids*. 1995;30:513-519

630   33.   Aldenderfer M. Moving up in the world: Archaeologists seek to understand

631   how and when people came to occupy the andean and tibetan plateaus. *Am Sci*.

632   2003;91:542-529

633   34.   Beall CM. Two routes to functional adaptation: Tibetan and andean high-

634   altitude natives. *Proc Natl Acad Sci U S A*. 2007;104 Suppl 1:8655-8660

635   35.   Heather LC, Cole MA, Tan JJ, Ambrose LJ, Pope S, Abd-Jamil AH, Carter

636   EE, Dodd MS, Yeoh KK, Schofield CJ, Clarke K. Metabolic adaptation to

637   chronic hypoxia in cardiac mitochondria. *Basic Res Cardiol*. 2012;107:268

638   36.   Ashrafian H, O'Flaherty L, Adam J, Steeples V, Chung YL, East P,

639   Vanharanta S, Lehtonen H, Nye E, Hatipoglu E, Miranda M, Howarth K,

640   Shukla D, Troy H, Griffiths J, Spencer-Dene B, Yusuf M, Volpi E, Maxwell

641   PH, Stamp G, Poulsom R, Pugh CW, Costa B, Bardella C, Di Renzo MF,

642   Kotlikoff MI, Launonen V, Aaltonen L, El-Bahrawy M, Tomlinson I, Pollard

643   PJ. Expression profiling in progressive stages of fumarate-hydratase

644   deficiency: The contribution of metabolic changes to tumorigenesis. *Cancer*

645   *Res*. 2010;70:9153-9165

646 37. Berg JM, Tymoczko JL, Stryer L. Glycolysis. *Biochemistry*. 2002.

647 38. Mora A, Davies AM, Bertrand L, Sharif I, Budas GR, Jovanovic S, Mouton V,

648   Kahn CR, Lucocq JM, Gray GA, Jovanovic A, Alessi DR. Deficiency of pdk1

649   in cardiac muscle results in heart failure and increased sensitivity to hypoxia.

650   *EMBO J*. 2003;22:4666-4676

651 39. Papandreou I, Cairns RA, Fontana L, Lim AL, Denko NC. Hif-1 mediates

652   adaptation to hypoxia by actively downregulating mitochondrial oxygen

653   consumption. *Cell Metab*. 2006;3:187-197

654

655

Table 1: Nuclear genes encoding mitochondrial proteins: the twenty 'most selected' (i.e. smallest GWADS p-values) in Tibetan high-altitude natives

Entrez ID	Gene name	GWADS min P	Reaction
5230	'PGK1'	0.000427922	'PGK'
5211	'PFKL'	0.000562071	'PFK'
4696	'NDUFA3'	0.001056733	'NADH2-u10m'
34	'ACADM'	0.002100322	All 'FAOX'
435	'ASL'	0.003329005	'ARGSL'
539	'ATP5O'	0.003329005	'ATPS4m'
27068	'PPA2'	0.004127063	'PPAm'
2937	'GSS'	0.004425362	'GTHS'
8170	'SLC14A2'	0.004892165	'UREAt'
4715	'NDUFB9'	0.005012697	'NADH2-u10m'
7991	'TUSC3'	0.005679664	'NADH2-u10m'
3145	'HMBS'	0.006801907	'HMBS'
10476	'ATP5H'	0.008432045	'ATPS4m'
4709	'NDUFB3'	0.00856278	'NADH2-u10m'
50	'ACO2'	0.008803353	'ACONTm'
2271	'FH'	0.008830507	'FUMm'
1350	'COX7C'	0.01011429	'CompIVr1'
4697	'NDUFA4'	0.01011429	'NADH2-u10m'
210	'ALAD'	0.010792961	'PPBNGS'
23761	'PISD'	0.011201573	'PSDm'

Table 2: Metabolites with the largest positive shadow prices when optimising the mitochondrial metabolic network for either haeme or ATP synthesis (and corresponding reactions)

Optimize haeme synthesis			Optimize ATP synthesis		
Metabolite	*Shadow price*	*Reaction(s)*	*Metabolite*	*Shadow price*	*Reaction(s)*
c204(c)	1.30	C204 (1)§, C204t (1)	fdp(c)	4	**PFK*** (1), FBA (2)
c204coa(c)	1.30	C204, C204CRN1 (1), C204CRN3 (1)	f6p(c)	3	**PFK***, PGI (3)
c204crn(c)	1.30	C204CRN1, C204CRN2 (1)	g6p(c)	3	HEX1 (4), PGI, G6PI#
c204coa(m)	1.30	C204CRN3, **FAOXC204***#	13dpg(c)	2.20	**PGK*** (5), GAPD (6)
c204crn(m)	1.30	C204CRN2, C204CRN3	c204coa(c)	2	C204 (7), C204CRN1 (8), C204CRN3 (9)
pheme(m)	1.00	FCLTm (6)	c204crn(c)	2.00	C204CRN1, C204CRN2 (10)
ppp9(m)	1.00	PPPGOm (6), FCLTm,	dhap(c)	2.00	TPI (11), FBA, G3PDm (12)
pppg9(c)	0.86	CPPPGO (8), PPPG9tm (8)	g3p(c)	2.00	FBA, G3PATm (13), G3PDm, GAPD, TPI
pppg9(m)	0.86	PPPG9tm, PPPGOm,	glc-D(c)	2.00	GLCt1 (14), HEX1
cpppg3(c)	0.76	CPPPGO, UPPDC1 (9)	c204coa(m)	2.00	C204CRN3, **FAOX204***#
hmbil(c)	0.76	**HMBS*** **(10)**, UPP3S (11)	c204crn(m)	2.00	C204CRN2, C204CRN3
uppg3(c)	0.76	UPP3S, UPPDC1	2pg(c)	1.19	ENO, PGM,
ppbng(c)	0.19	**HMBS***, **PPBNGS*** **(12)**	3pg(c)	1.19	**PGK***, PGM
5aop(c)	0.10	**PPBNGS***, 5AOPtm (13)	pep(c)	1.19	PYK, CITtbm
5aop(m)	0.10	5AOPtm, ALASm (14)	succoa(m)	0.81	AKGDm, ALASm#, OCOAT1m#
succoa(m)	0.10	AKGDm (15), ALASm, OCOAT1m#	akg(c)	0.62	ICDHxm (20), ICDHym#, TYRTAm#, AKGDm
13dpg(c)	0.05	**PGK*** (16), GAPD (17)			

2pg(c)'	0.0476 19048	ENO, PGM,			
13dpg(c)	0.0476 19048	**PGK***, GAPD			

§Bracketed numbers are reaction rank based on metabolite shadow price
#Flux through this reaction was zero
*Corresponding gene is one of the 'twenty most selected' in Table 1

Table 3: Reactions with the smallest relative flux spans when optimising the mitochondrial metabolic network for either **a:** haeme synthesis or **b:** ATP synthesis

a. Optimize haeme synthesis[#]			b. Optimize ATP synthesis		
Reaction	Relative flux span ($\times 10^{-6}$)	Rank	Reaction	Relative flux span ($\times 10^{-6}$)	Rank
CompIVr1*	1.2	1	ATPtm	0.01	1
CYOR-u10m	1.2	1	**CompIVr1***	0.10	2
NADH2-u10m*	1.3	3	CYOR-u10m	0.10	3
CPPPGO	1.4	3	SUCOASm	0.20	4
FCLTm	1.4	3	ENO	0.21	5
FE2t1	1.4	3	GAPD	0.21	6
FE2tm	1.4	3	**PGK***	0.21	7
HMBS*	1.4	3	PGM	0.21	8
PPPG9tm	1.4	3	FBA	0.21	9
UPP3S	1.4	3	GLCt1	0.21	10
UPPDC1	1.4	3	HEX1	0.21	11
PPPGOm	1.4	3	**PFK***	0.21	12
5AOPtm	1.4	3	PGI	0.21	13
AKGDm	1.4	3	TPI	0.21	14
ALASm	1.4	3	**ACONTm***	0.22	15
ASPGLUm	1.4	3	AKGDm	0.22	16
ASPTAm	1.4	3	CSm	0.22	17
GLYt2r	1.4	3	ICDHxm	0.22	18
GLYtm	1.4	3	**NADH2-u10m***	0.27	19
MDHm	1.4	3	**FUMm***	0.29	20
PPBNGS*	1.4	3			

[#]21 reactions due to 'drawn ranking'
*Corresponding gene is one of the 'twenty most selected' in Table 1

Constraint-based mitochondrial modelling, hypoxia and human genetics

A   **B**   **A**   **B**   **A**   **B**

First pair (left):

EXCHANGE REACTIONS:
'EX_12dgr_m(e)', 'Ex_acac', 'EX_c204(e)', 'EX_c226(e)', 'EX_co2(e)', 'EX_coa(e)', 'EX_cys-L(e)', 'EX_fe2(e)', 'EX_glc(e)', 'EX_glu-L(e)', 'EX_gly(e)', 'EX_glyc(e)', 'EX_glyc3p(e)', 'EX_h(e)', 'EX_h2o(e)', 'Ex_hb(e)', 'EX_hdca(e)', 'EX_lac-L(e)', 'EX_o2(e)', 'EX_ocdca(e)', 'EX_ocdcea(e)', 'EX_ocdcya(e)', 'EX_pi(e)', 'EX_ps_m(e)', 'EX_urea(e)'

GLYCOLYSIS:
'GLCt1', 'HEX1', 'G6PI', 'G6PI2', 'PGI', 'PFK', 'FBA', 'TPI', 'GAPD', 'PGK', 'PGM', 'ENO', 'PYK', 'LDH_L', 'L-LACt2r'

TCA CYCLE:
'PYRt2m', 'PDHm', 'PCm', 'ME2m', 'CSm', 'ACONTm', 'ICDHxm', 'ICDHym', 'AKGDm', 'SUCOASm', 'SUCD1m', 'FUMm', 'MDHm'

OXPHOS:
'COAr', 'COAtm', 'CO2r', 'CO2m', 'GTPtm', 'NDPK1', 'SUCCt2m', 'FRDcm', 'MALtm', 'NADH2-u10m', 'SUCD3-u10m', 'CompIVr1', 'CYOOm3', 'ATPS4m', 'ATPtm', 'PIt2r', 'PIt2m', 'H2OD'

Middle pair:

OXIDATIVE STRESS:
'H2Ot', 'H2Otm', 'SPODMm', 'CATm', 'CYSt2r', 'GLUCYS', 'GLUt2r', 'GLYt2r', 'GTHDHm', 'GTHOm', 'GTHPm', 'GTHRDt', 'GTHS'

BETA OX:
'FAOXC160', 'FAOXC180', 'FAOXC181', 'FAOXC182', 'FAOXC204', 'FAOXC226'

FA TRANSPORT/ACTIVATION:
'HDCAr', 'OCDCAr', 'OCDCEAr', 'OCDCYAr', 'C160', 'C160CPT1', 'C160CPT2', 'C160CRN', 'C180', 'C180CPT1', 'C180CPT2', 'C180CRN', 'C181', 'C181CRN1', 'C181CRN2', 'C181CRN3', 'C182', 'C182CRN1', 'C182CRN2', 'C182CRN3', 'C204', 'C204CRN1', 'C204CRN2', 'C204CRN3', 'C204t', 'C226', 'C226CRN1', 'C226CRN2', 'C226CRN3', 'C226t'

UREA CYCLE:
'ASPGLUm', 'ASPTA', 'ASPTAm', 'AKGMALtm', 'MDH', 'GLUDx', 'GLUDy', 'GLUt2m', 'GLUt2r', 'NH4mt', 'CBMKm', 'OCBTm', 'CITRm', 'ARGSS', 'ARGSL', 'ARGN', 'ORNt3m', 'ORNt4m', 'UREAt', 'GLYt2r', 'GLYtm', 'GLYAMDTR', 'GACMTR'

Right pair:

PHOSPHOLIPID BIOSYNTHESIS:
'CK', 'DM_phoslipid(m)', 'CITRm', 'DAGCPTm', 'PCtm', 'PCHOLPm', 'DAGKm', 'PAPAm', 'DASYNm', 'PGSAm', 'PGPPm', 'CLPNSm', 'AGATm', 'G3PATm', 'FASYNm', 'G3PDm', 'GLYC3Ptm', 'GLYC3Pt1', 'GLYKm', 'GLYCtm', 'PSDm', 'PSt', 'PStm', '12DGRt1', 'ETHAPTm'

'MMSAD1m', 'PPCOACm', 'TYRTAm', 'HACDm'

KETONES:
'ACACr', 'ACACtm', 'ACACT1m', 'BDHm', 'OCOAT1m', 'HMGCOASm', 'HMGLm'

HAEME BIOSYNTHESIS:
'DM_heme(m)', 'GLYCtm', 'ALASm', '5AOPtm', 'PPBNGS', 'HMBS', 'UPP3S', 'UPPDC1', 'CPPPGO', 'PPPG9tm', 'PPPGOm', 'FCLTm', 'FE2t1', 'FE2tm'

NUCLEOTIDE METABOLISM:
'TMDK1m', 'DGNSKm', 'ADK1', 'ADK1m', 'ADK4m', 'DUTPDPm', 'GHMT2rm', 'FTHFLm', 'THFATm', 'PPA', 'PPAm', 'CITtam', 'CITtbm', 'PEPCKm', 'H2CO3Dm', 'HCO3Em', 'ATPCTP'

35

Figure 1: Heatmap showing the effect of hypoxia on flux distribution in the mitochondrial metabolic network. Red = flux increased by > 0.1 U; green = flux decreased by > 0.1 U; yellow = flux changed by < 0.1 U..**A:** Flux balance analysis, with ATP synthesis as the objective function. **B:** Uniform random sampling. (U = μm min^{-1} g^{-1})
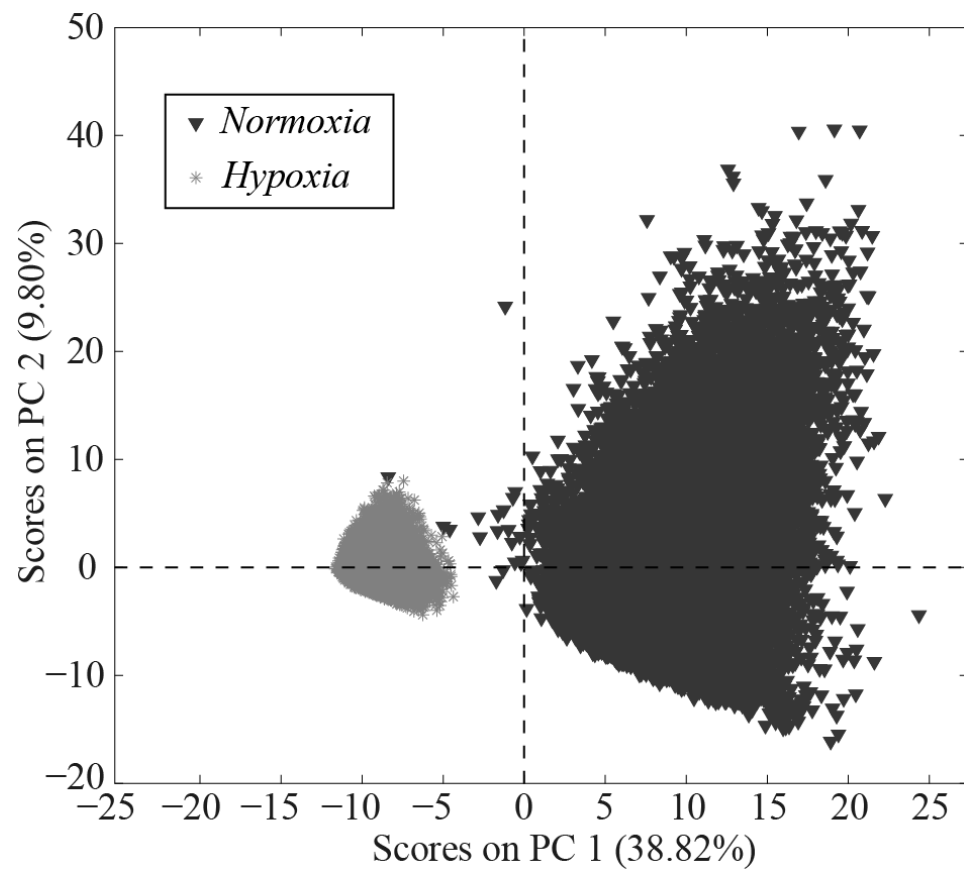
Figure 2: Biplot showing scores on principal component 1 vs. scores on principal component 2. Both components are from a five-component PCA model of data sampled in hypoxia and normoxia. Black triangles = normoxia; grey stars = hypoxia.